CrossMark

Moving Magnetic Features Around a Pore

A. J. Kaithakkal[1], T. L. Riethmüller[1], S. K. Solanki[1,2], A. Lagg[1], P. Barthol[1], A. Gandorfer[1], L. Gizon[1], J. Hirzberger[1],
M. vanNoort[1], J. Blanco Rodríguez[3], J. C. Del Toro Iniesta[4], D. Orozco Suárez[4], W. Schmidt[5],
V. Martínez Pillet[6], and M. Knölker[7,8]

[1] Max Planck Institute for Solar System Research, Justus-von-Liebig-Weg 3, Göttingen D-37077, Germany; anjali@mps.mpg.de
[2] School of Space Research, Kyung Hee University, Yongin, Gyeonggi, 446-701, Korea
[3] Grupo de Astronomía y Ciencias del Espacio, Universidad de Valencia, E-46980 Paterna, Valencia, Spain
[4] Instituto de Astrofísica de Andalucía (CSIC), Apartado de Correos 3004, E-18080 Granada, Spain
[5] Kiepenheuer-Institut für Sonnenphysik, Schöneckstr. 6, D-79104 Freiburg, Germany
[6] National Solar Observatory, 3665 Discovery Drive, Boulder, CO 80303, USA
[7] High Altitude Observatory, National Center for Atmospheric Research, P.O. Box 3000, Boulder, CO 80307-3000, USA

Abstract

Spectropolarimetric observations from SUNRISE/IMaX, obtained in 2013 June, are used for a statistical analysis to determine the physical properties of moving magnetic features (MMFs) observed near a pore. MMFs of the same and opposite polarity, with respect to the pore, are found to stream from its border at an average speed of 1.3 km s^{-1} and 1.2 km s^{-1}, respectively, with mainly same-polarity MMFs found further away from the pore. MMFs of both polarities are found to harbor rather weak, inclined magnetic fields. Opposite-polarity MMFs are blueshifted, whereas same-polarity MMFs do not show any preference for up- or downflows. Most of the MMFs are found to be of sub-arcsecond size and carry a mean flux of $\sim 1.2 \times 10^{17}$ Mx.

1. Introduction

The presence of moving magnetic features (MMFs) around sunspots was first noted by Sheeley ([1969](#)), who found that there are small-scale bright features moving out radially from mature sunspots with speeds of about 1 km s^{-1}. Later, Harvey & Harvey ([1973](#)) found that these moving bright features are magnetic and named them MMFs. The majority of the studies on MMFs in the literature was focused on proving the connection between penumbral magnetic fields and the origin of MMFs (Zhang et al. [2003](#); Sainz Dalda & Martínez Pillet [2005](#); Cabrera Solana et al. [2006](#); Kubo et al. [2007a](#), [2007b](#); Zhang et al. [2007](#), and references therein), under the assumption that a penumbra is necessary for MMFs to be produced. However, Harvey & Harvey ([1973](#)) showed that a penumbra is not essential for the presence of MMFs. Later studies have confirmed that MMFs are observed around sunspots without a penumbra—or more precisely, pores (Zuccarello et al. [2009](#); Criscuoli et al. [2012](#); Verma et al. [2012](#)).

Studies have further shown that MMFs appear as either unipolar magnetic features or bipolar feature pairs. The unipolar MMFs can have either the same or opposite polarity, with respect to the parent spot (Shine & Title [2001](#)). Their typical size is below $2''$, and they exhibit a broad range of horizontal velocity from 0.1 to 1.5 km s^{-1} (Harvey & Harvey [1973](#); Brickhouse & Labonte [1988](#); Zhang et al. [2003](#)). Unipolar features with opposite polarity to the spot are reported to have higher speeds than features that are parts of bipolar pairs or unipolar features with the same polarity as the spot (for a review on MMFs see Hagenaar & Shine [2005](#)).

A recent study by Criscuoli et al. ([2012](#)), using data from IBIS at NSO/DST, which investigated six unipolar MMFs around a pore, out of which three were of opposite polarity to the pore, confirmed that opposite-polarity MMFs move faster than same-polarity MMFs. Furthermore, MMFs of opposite polarity were shown to be associated with upflows, whereas those of the same polarity as the pore were found to be associated with downflows. The authors also pointed out that the characteristics of MMFs observed around a pore are generally consistent with those obtained for MMFs around sunspots.

Despite the existing studies on MMFs, it is not yet clear to what extent the origin of MMFs is related to the presence of a penumbra. Also, there are very few studies that provide information on the physical properties of the MMFs. In this paper, we present a statistical analysis of physical properties of MMFs observed near a pore. We used high spatial resolution ($\sim 0''.15$) and high-cadence (36.5 s) spectropolarimetric data obtained during the second flight of the balloon-borne observatory SUNRISE (Solanki et al. [2010](#), [2017](#); Barthol et al. [2011](#); Berkefeld et al. [2011](#); Gandorfer et al. [2011](#)) for our analysis.

2. Observation and Data Analysis

The field of view (FOV) of IMaX/ SUNRISE II observations, carried out on 2013 June 12, 23:39–23:55 UT, covered a large pore that is part of the active region AR 11768 ($\mu = 0.93$; see Figure [1](#)). IMaX recorded the full Stokes vector over the Fe I 5250.2 Å (Landé factor, $g = 3$) spectral line in the V8-4 mode (for details, see Martínez Pillet et al. [2011a](#)), i.e., at seven wavelength positions ($\lambda = \pm 120, \pm 80, \pm 40$ mÅ, and the line center) within the line, and one in the nearby continuum ($+227$ mÅ). The FOV of the images is $51'' \times 51''$ with a scale of $0''.0545$ per pixel.
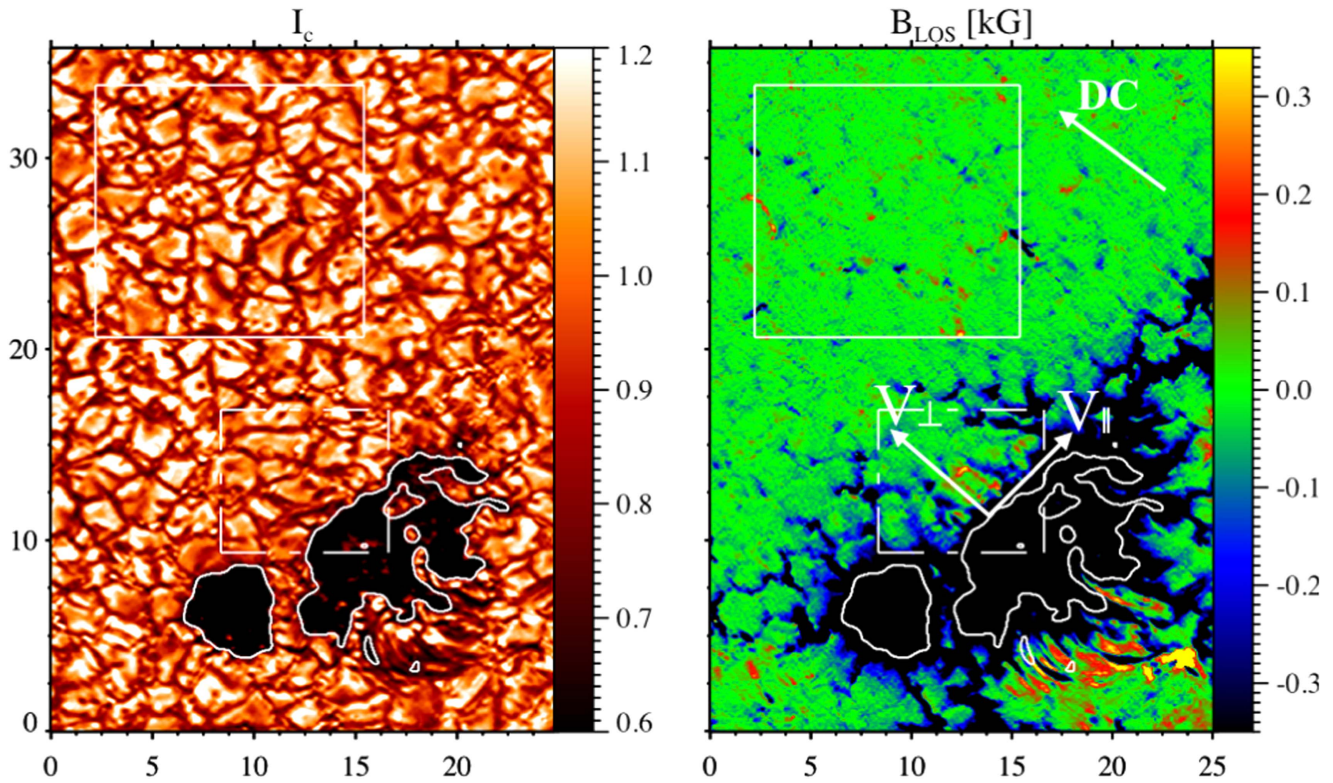

Figure 1. Left: normalized continuum intensity map of the first frame of the analyzed time series. Right: corresponding $B_{\rm LOS}$ map, saturated to ±350 G, where $V_\perp$ and $V_\parallel$ represent components perpendicular and parallel to the pore boundary, respectively, of the proper motion velocity of the MMFs. The white box on the upper left corner indicates the quite-Sun region. The white dashed box outlines our region of interest (ROI). The white contours outlining the edges of the pores represent the continuum intensity level of $0.69\,I_{c,\rm QS}$, where $I_{c,\rm QS}$ is the continuum intensity averaged over the quite-Sun region. DC corresponds to disk center, and the arrow point toward the approximate disc center direction. The axes are in arcseconds.

The images were corrected for dark current, flat field, fringes, polarization crosstalk, and stray light. Afterward, the data were reconstructed with the help of a point-spread function retrieved from inflight phase-diversity measurements. The reconstructed IMaX data have a spatial resolution of $0''\!.15$–$0''\!.18$. The noise (σ) in Stokes V is around $7 \times 10^{-3}I_c$, where I_c is the continuum intensity. The Stokes vectors were inverted using the classical SPINOR code (Frutiger et al. 2000), which uses the STOPRO routines (Solanki 1987), assuming a single-component model atmosphere. The inversion was set to return the temperature at three optical depths, and height-independent magnetic field parameters (B, γ and ϕ), line-of-sight (LOS) velocity ($v_{\rm LOS}$), and microturbulent velocity. We correct $v_{\rm LOS}$ for the blueshift across the FOV due to the collimated setup of the Fabry–Pérot etalon. More details on the data reduction and inversions are provided by Solanki et al. (2017) and references therein. The signature of p-modes was removed from the continuum and $v_{\rm LOS}$ maps using a subsonic filter (Title et al. 1989) with a cut-off phase velocity of $4\,{\rm km\,s}^{-1}$. The zero (reference) point for $v_{\rm LOS}$ maps is defined as the spatio-temporal average value within the quiet-Sun region in the FOV (region within the solid white box in Figure 1) and subtracted from all the frames. The continuum intensity maps are normalized with respect to the mean quiet-Sun value. Image sequences of all the relevant parameters were corrected for rotation of the FOV caused by the alt-azimuth mounting of the Sunrise telescope, then aligned using a spatial cross-correlation technique. We then chose a small area (denoted by the dashed white square in Figure 1) with a size of $8''\!.3 \times 7''\!.5$ as our region-of-interest (ROI).

3. Identification and Tracking of MMFs

MMFs were identified by applying a modified version of the multilevel tracking (MLT) algorithm of Bovelet & Wiehr (2001) to maps of the LOS component of the magnetic field vector, $B_{\rm LOS}$. MLT uses multiple threshold levels with decreasing values of $B_{\rm LOS}$. The area of the feature grows with lower thresholds. If the separation between two given features identified by two consecutive thresholds is less than three pixels, they are joined into a single feature. The process of identifying and separating the features based on the thresholds was repeated until the lowest threshold level was reached. After a number of trials, we chose 40 thresholds ranging from 500 to 40 G (the latter is the 3σ value obtained from the $B_{\rm LOS}$ maps). The code returned spatial locations of the features, each of which was tagged with a unique identification number based on its polarity. We then calculated the magnetic centroid of each feature, which is defined as the average of the position (x_i, y_i) weighted by $B_{\rm LOS}(x_i, y_i)$. We selected those features that (1) have a minimum size of five pixels (0.1 Mm in diameter); (2) have a per-pixel $B_{\rm LOS}$ value greater than 40 G; and (3) are within 3 Mm distance from the visible pore boundary. The visible boundary of the pore is defined as that where I_c is 69% of the quiet-Sun value. It should be noted that the magnetic boundary of the pore is larger than its visible boundary. For simplicity, we henceforth refer to the visible pore boundary/border as the pore border/boundary.

MMFs were tracked using spatial overlap (Iida et al. 2012) over consecutive $B_{\rm LOS}$ maps assuming a maximum advection velocity of $4\,{\rm km\,s}^{-1}$ (corresponding to a displacement of 4 IMaX pixels within 36.5 s). If there were multiple features in
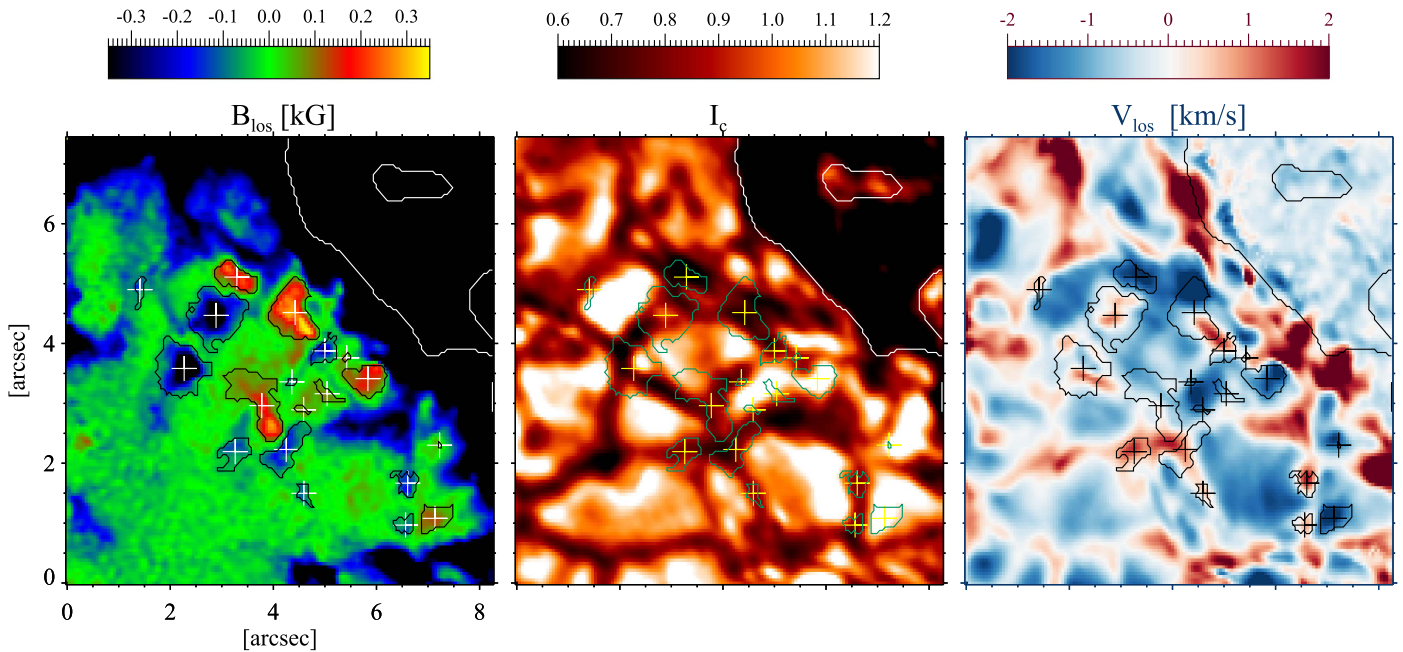
Figure 2. Left to right: B_{LOS}, $I_c/\langle I_{c,QS}\rangle$, and v_{LOS} maps of our ROI taken at three minutes after the start of the observation (please note that the image is reversed in the vertical direction with respect to the image in Figure 1). The white contour outline, the pore border, and the black contours (green in central panel) enclose the chosen features. The + signs represent the magnetic centroid positions of the MMFs.

(An animation of this figure is available.)

the successive frame that spatially overlap with a given feature from the previous frame, the one with the minimum difference in flux with respect to the given feature was chosen. From the MMFs selected from the MLT method, only those with a minimum life time of four frames (2.4 minutes) were chosen. In total, we selected 88 MMFs that satisfy all the above conditions. We then obtained values of all relevant parameters (such as field strength (B), inclination (γ), normalized continuum intensity, etc.) at the magnetic centroid position. Further, we calculated the perpendicular ($V_\perp$) and parallel ($V_\parallel$) components (the direction being defined with respect to the pore border) of the proper motion velocity of the MMFs (see right panel of Figure 1). Figure 2 shows B_{LOS} ($=B\cos\gamma$), $I_c/\langle I_{c,QS}\rangle$, and v_{LOS} maps, taken at three minutes after the start of the observation, of our ROI with contours outlining MMFs we selected.

4. Results

We identified 44 opposite and 44 same-polarity MMFs. From a visual inspection of the transverse field maps in the region, we find horizontal fields pointing from some of the opposite-polarity MMFs to the same-polarity MMFs, suggesting that the two form an MMF pair. As these MMFs are surrounded by many other neighboring MMFs, it is difficult to follow them as pairs. Hence, we treated them as individual MMFs to obtain their physical properties. Nevertheless, the possible connection of these MMF-pairs would be worth looking into in more detail as part of future studies.
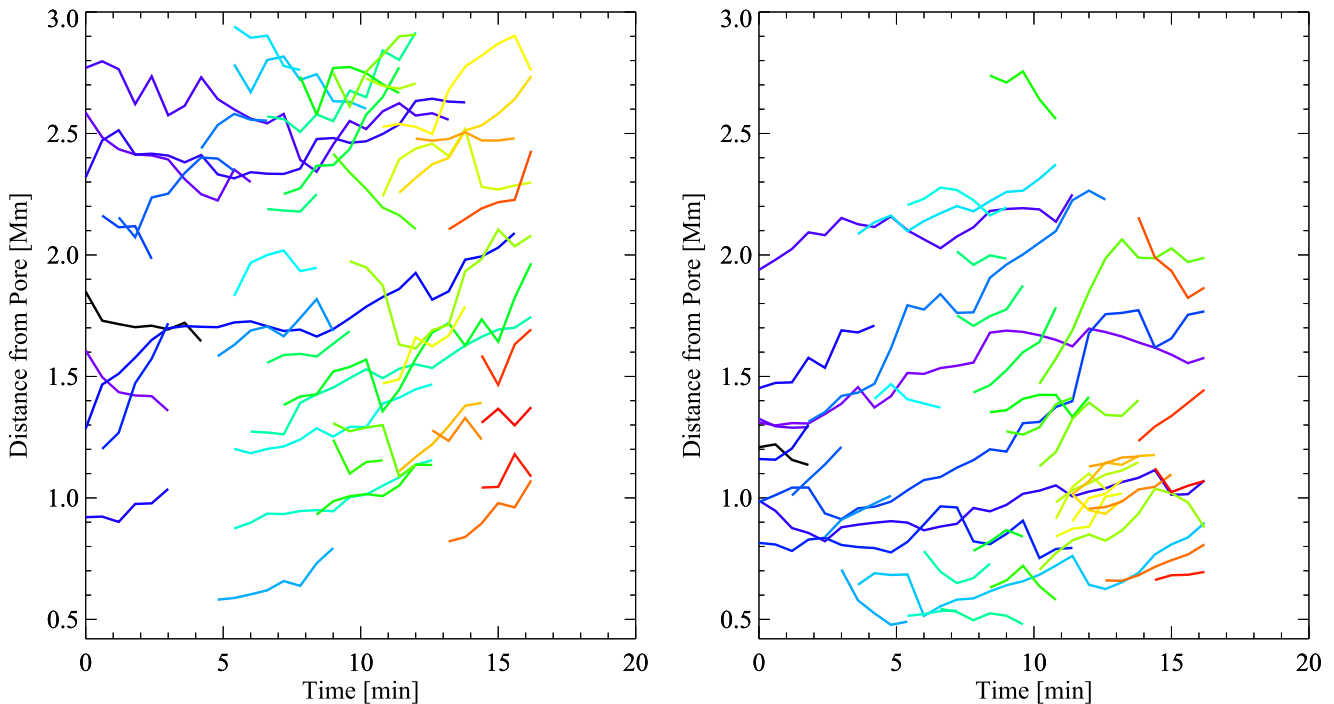
Figure 3 presents the variation of the minimum distance of the magnetic centroid of the MMFs from the pore border with time. It shows that, for the majority of the MMFs of both polarities, the minimum distance from the boundary of the pore increases with time. When first identified, a few of the MMFs were as close to the pore border as 0.6 Mm. We find that, closer to the pore, MMFs of opposite polarity dominate. The number

of opposite-polarity MMFs within a distance of 1.5 Mm from the pore boundary is twice that of the same-polarity MMFs. It is possible that the strong magnetic field of the pore is masking the same-polarity MMFs closer to the pore, thereby rendering them less visible. As described by Criscuoli et al. (2012) same-polarity MMFs could be detected when they are not embedded in the ambient field of the pore.

The angular distribution of the path followed by the MMFs shows a broad peak in the range [150°–180°], where 180° represents motion in radial outward direction. Thus, although the MMFs are buffeted by the granulation, their motion is not a pure random walk. We find that some of these MMFs move in a tangential direction to the pore boundary, whereas some others exhibit a random direction of motion for some period during their observed lifetime. However, most of the MMFs (72%) eventually move away from the pore border. As we do not find any difference in the physical properties between MMFs based on the path they follow, we did not differentiate between them when presenting our results in the following.

For each MMF, relevant physical parameters at the magnetic centroid position were determined, and then those values were averaged over the period for which the MMF was observed. However, the whole feature was considered for the calculation of magnetic flux and area. We estimated the magnetic flux of each MMF as $\phi = B_{LOS} A$, where B_{LOS} represents the LOS component of the magnetic field vector, and A is the area of the resolution element.

We averaged magnetic flux and area over the time for which each MMF could be tracked. For MMFs of both polarities, the area distribution is in the range 0.01–0.5 Mm^2 (i.e., the smallest ones are close to the spatial resolution of the SUNRISE/IMaX observations) and the mean area is about 0.1 Mm^2. The magnetic flux distribution of the opposite-polarity MMFs lies in the range 7.7×10^{15}–9.5×10^{17} Mx, with the mean flux being 1.16×10^{17} Mx. For the same-polarity MMFs, the

Figure 3. Left: variation of the minimum distance from the pore border with time for the same-polarity MMFs. Right: same as the left panel, but for opposite-polarity MMFs. Different colors represent tracks of different MMFs.

magnetic flux distribution ranges from 5.8×10^{15} to 6.6×10^{17} Mx, with a mean value of 1.19×10^{17} Mx.

Distributions of B, γ, v_{LOS}, $V_{\perp}$ and $I_c/\langle I_{c,\mathrm{QS}}\rangle$ averaged over the observed period of the MMFs corresponding to the magnetic centroid position are shown in Figure 4. The details of the same are presented below:

(1) For MMFs of both polarities, the intrinsic field strength (Figure 4(a)) displays a broad distribution: for opposite-polarity MMFs, it is in the range 250–1300 G; for the same-polarity MMFs, it is in the range 250–900 G. We also find that, as the distance from the pore border increases, the field strength decreases for MMFs of both types (correlation coefficients are -0.60 and -0.50, respectively, for opposite- and same-polarity MMFs). However, the field strength displays random fluctuations with time for MMFs of both polarities.

(2) The histograms of field inclinations (Figure 4(b)) show that MMFs of both polarities are highly inclined. The mean inclination of opposite polarity MMFs is about 75° and that of same-polarity MMFs is about 106°. With increasing distance from the pore boundary, the magnetic field displays a tendency to become more vertical for MMFs of opposite polarity (correlation coefficient: -0.46), whereas this trend is comparatively weak for the same-polarity MMFs. These observations are in line with the study on unipolar MMFs around a pore by Criscuoli et al. (2012), who showed that field vectors of MMFs can be highly inclined, although a vertical orientation is the most probable configuration. They also reported that, for both types of the MMFs, the field becomes more vertical with increasing distance from the pore border.

(3) The distributions of v_{LOS} (Figure 4(c)) show that MMFs of opposite polarity are characterized by preferential upflows. The peak of the distribution is around 1 km s^{-1}

and the mean value is $\sim$1.1 km s^{-1}. In contrast, the same-polarity MMFs are (on average) unshifted. Opposite-polarity MMFs exhibit a slow decrease in upflow as their distance from the pore border increases (correlation coefficient: 0.68). Some MMFs of both polarities show both up- and downflows during their lifetime.

This result agrees partly with that of Criscuoli et al. (2012). The authors show that opposite-polarity MMFs are associated with upflows and same-polarity MMFs with downflows. They also found that the upflows associated with the opposite-polarity MMFs decrease slowly with distance from the pore border.

(4) Panel (d) of Figure 4 presents the histograms of the perpendicular component of the proper motion velocity ($V_{\perp}$) of the MMFs. MMFs of opposite polarity have speeds in the range [-4.7 to 3.4] km s^{-1}. They move away from the pore border with a mean speed of $\sim$1.2 km s^{-1}. The mean speed of these MMFs was $\sim$1.5 km s^{-1} when first detected and was $\sim$1.1 km s^{-1} when they were recognized for the last time. The mean speed of the opposite-polarity MMFs that move toward the pore is $\sim$$-2.0$ km s^{-1}.

MMFs of same polarity have $V_{\perp}$ in the range of [-2.5 to 3.7] km s^{-1}. They move away from the pore with a mean speed of 1.3 km s^{-1}. The mean value of $V_{\perp}$ corresponding to the first and last detection of these MMFs is $\sim$2.2 and 1.2 km s^{-1}, respectively. The same-polarity MMFs that move toward the pore have a mean speed of $\sim$$-1.1$ km s^{-1}.

The mean initial speed with which the MMFs of both polarities move away from the pore is close to the value of 1.8 km s^{-1} found by Hagenaar & Shine (2005), using MDI data in the high-resolution mode. The mean $V_{\perp}$ value of the MMFs that move away is higher than the value of 0.45 km s^{-1} reported by Zhang et al. (2003) and
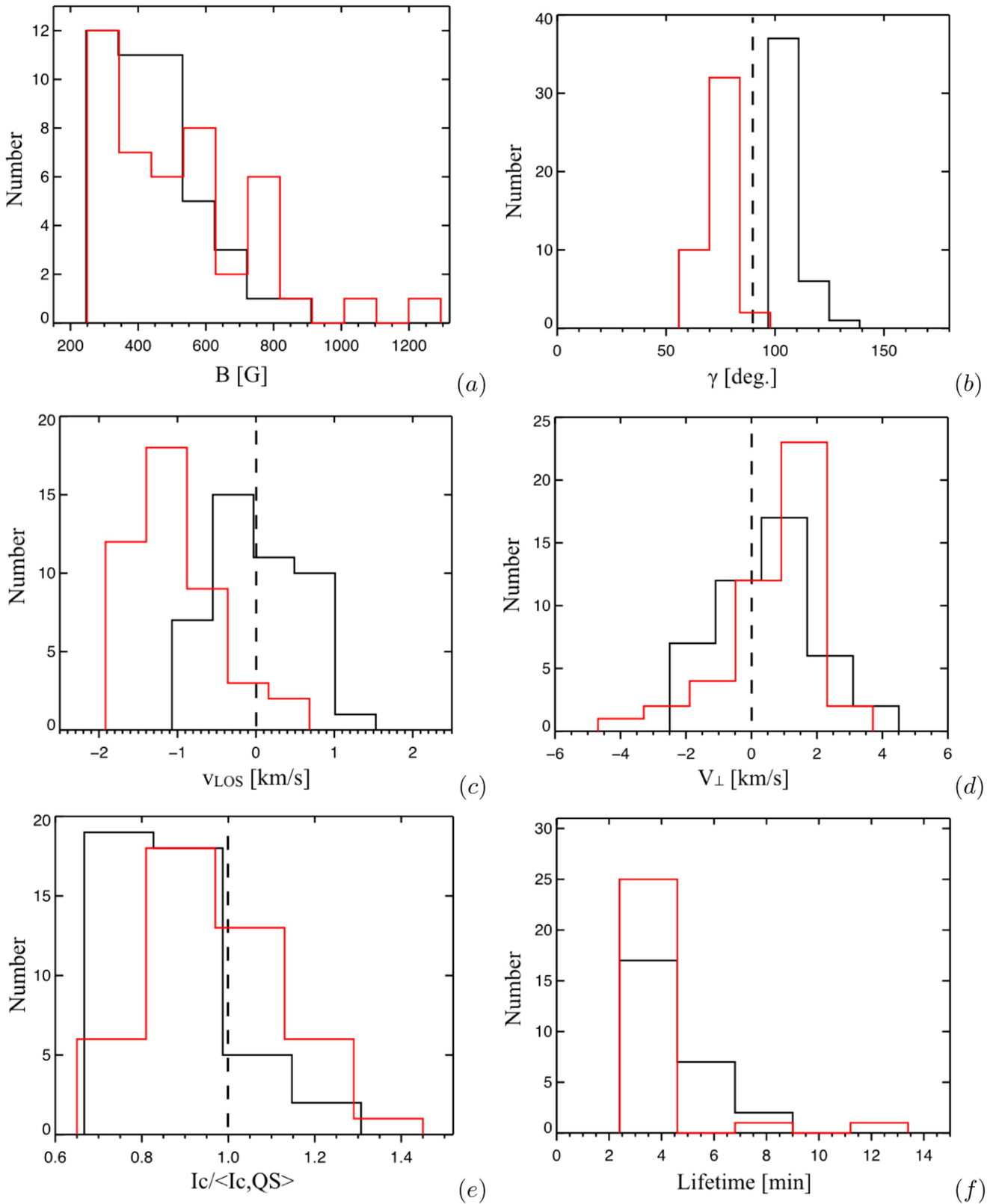
Figure 4. Histograms of the lifetime average of B (a), γ (b), v_{LOS} (c), $V_\perp$ (d) (see the right panel of Figure 1 for definition), at the magnetic centroid position (e) and, lifetime of MMFs (f). Red (black) plots represent opposite- (same-) polarity MMFs. In panel (c), negative Doppler velocities correspond to blueshifts. In panel (d), positive velocities represent MMFs moving away from the pore border, and negative velocities represent MMFs moving toward the pore.

of $0.34\,\mathrm{km\,s^{-1}}$ obtained by Kubo et al. (2007b) for MMFs around sunspots, both using MDI data. For bipolar MMFs observed around a sunspot without penumbra (using Hinode data), Zuccarello et al. (2009) found that the MMFs have a typical horizontal velocity of $0.7\,\mathrm{km\,s^{-1}}$.

Table 1
Comparison of the Physical Parameters of MMFs Obtained in this Study to Some Found in the Literature

Reference	Instrument	Mean Flux (Mx)	B (G)	γ (degree)	v_{LOS} (km s^{-1})	Mean Horizontal Velocity[a] (km s^{-1})
This study	SUNRISEII/IMaX	1.16×10^{17}	250–1300	55–85	upflow	1.2
		1.19×10^{17}	250–900	97–128	no preference	1.3
Criscuoli et al. (2012)	DST/IBIS	⋯	500–1700	10–50	upflow	∼1
		⋯	″	120–160	downflow	⋯
Kubo et al. (2007b)	ASP and MDI	⋯	300–1600	40–70	⋯	0.34
		⋯	″	90–170	⋯	″
Zhang et al. (2003)	MDI	3.6×10^{18}	⋯	⋯	⋯	0.45

Notes. For each study except Kubo et al. (2007b), parameters in the first line are for opposite-polarity MMFs and those in the second line are for same-polarity MMFs. For the study by Kubo et al. (2007b), the first line represents values for same-polarity MMFs.
[a] For our study, a mean value of $V_\perp$ (perpendicular component of proper motion velocity) of MMFs moving outward is given.

For MMFs of opposite polarity, $V_\parallel$ is in the range of [−4.2 to 3.4] km s^{-1}, with a mean value of −0.17 km s^{-1}. The $V_\parallel$ of same-polarity MMFs also shows a broad range from −2.8 to 3.9 km s^{-1}, whereas the average value of the distribution is 0.12 km s^{-1}.

(5) Figure 4(e) shows that the majority of the same-polarity MMFs stays below the mean quiet-Sun intensity level. We find that the distribution has a broad range, with a mean value of 0.86. The opposite-polarity MMFs also exhibit a broad distribution ranging from 30% below the average quiet-Sun intensity to 40% above it, with a mean value of 0.97.

We find that, for MMFs of both polarities, the intensity varies randomly with time. For most of the same-polarity MMFs, the instantaneous intensity stays below the mean quiet-Sun value throughout their lifetime. In the case of opposite-polarity MMFs, the intensity is widely distributed over time.

(6) Histograms of the lifetime of the MMFs are presented in Figure 4(f). For these plots, we consider only those MMFs that were born and disappeared during the observation. Irrespective of the polarity, most of the MMFs have a lifetime of less than five minutes. The observed average lifetime of the same-polarity MMFs is about 4.1 minutes, and that of the opposite-polarity MMFs is 3.6 minutes.

5. Summary and Discussion

We investigated the physical properties of MMFs observed outside a pore using SUNRISEII/IMaX data. Our main results, obtained from the statistical analysis, are summarized as follows: MMFs of the same and opposite polarity to that of the pore are observed at one side of the pore boundary. Most of these MMFs are of sub-arcsecond size. The majority of the MMFs move away from the pore border with a preference for the radial direction. Opposite-polarity MMFs are generally blueshifted and same-polarity MMFs are (on average) unshifted. MMFs of both polarities are characterized by weak and inclined magnetic fields.

Although the motion of the MMFs we observed are greatly influenced by the granulation, they exhibit a clear preference for a radial outward motion. The tracks followed by the MMFs bear a resemblance to the trajectories of intergranular magnetic bright points (MBPs) reported by Jafarzadeh et al. (2014),

using SUNRISE/SuFI data (Gandorfer et al. 2011). Those authors demonstrated that the trajectories of the MBPs result from the superposition of random motions caused by granular evolution and intergranular turbulence, and systematic motions caused by steady granular evolution and mesogranular and supergranular flows. They also found that these MBPs are super-diffusive in nature. It would be worth investigating whether the MMFs show a similar dispersion trend.

We found that MMFs of both polarities are characterized by inclined magnetic fields, with most of them having field strengths below 1 kG. A study, based on ASP data by Kubo et al. (2007b) on MMFs around a sunspot, showed that many MMFs that are located on lines extrapolated from the horizontal component of the penumbra are associated with inclined magnetic fields with field strength below 1 kG. Criscuoli et al. (2012) found that the MMFs of both polarities observed around a pore have a wide distribution of magnetic field strengths ranging from 500 to 1700 G. The authors mention that the most probable value of B is above 1 kG and that the magnetic fields are most probably vertically oriented. The physical parameters of the MMFs obtained in this study are compared to those found by some other studies in Table 1.

MMFs of both polarities are found to be associated with inclined fields. However, with increasing distance from the pore border, they show a trend of becoming less inclined. If these are individual MMFs (i.e., not members of pairs), then it may have to do with the strong magnetic canopy of the pore, which forces the magnetic field of the MMFs to remain relatively horizontal. With increasing distance from the pore boundary, the canopy lies higher and the canopy field is weaker, so that, once they are far enough from the pore field, they become more vertical.

Our ROI is special when compared to other areas around the pore in that opposite-polarity MMFs prevail in this region. Figure 4(c) shows that opposite-polarity MMFs are preferentially associated with upflows. This picture is supported by the fact that the opposite-polarity MMFs are, on average, brighter than the same-polarity MMFs, although only around half the opposite-polarity MMFs are brighter than the average quiet-Sun. However, with increasing distance from the pore, these MMFs exhibit a slow decrease in blueshift, which implies that they possibly end up in the intergranular region just as the same-polarity MMFs.

The majority of the same-polarity MMFs are characterized by intensity values lower than the average quiet-Sun value. This suggests that most of these MMFs were born and

remained in the intergranular lanes. This is similar to the picture presented by Cameron et al. (2007). Using MHD simulations of a pore, the authors showed that intergranular lanes are preferentially occupied by features of the same polarity as the pore. This could be one reason why opposite-polarity MMFs are shorter-lived than the same-polarity ones; as the opposite-polarity MMFs move into the intergranular lanes, the chances are high that their magnetic flux is eventually cancelled out by the existing same-polarity flux. This could provide an explanation as to why same-polarity MMFs dominate the region beyond 2 Mm from the pore border.

Software: SPINOR (Frutiger et al. 2000), STOPRO (Solanki 1987).

References

Barthol, P., Gandorfer, A., Solanki, S. K., et al. 2011, SoPh, 268, 1
Berkefeld, T., Schmidt, W., Soltau, D., et al. 2011, SoPh, 268, 103
Bovelet, B., & Wiehr, E. 2001, SoPh, 201, 13
Brickhouse, N. S., & Labonte, B. J. 1988, SoPh, 115, 43
Cabrera Solana, D., Bellot Rubio, L. R., Beck, C., & del Toro Iniesta, J. C. 2006, ApJL, 649, L41
Cameron, R., Schüssler, M., Vögler, A., & Zakharov, V. 2007, A&A, 474, 261
Criscuoli, S., Del Moro, D., Giannattasio, F., et al. 2012, A&A, 546, A26
Frutiger, C., Solanki, S. K., Fligge, M., & Bruls, J. H. M. J. 2000, A&A, 358, 1109
Gandorfer, A., Grauf, B., Barthol, P., et al. 2011, SoPh, 268, 35
Hagenaar, H., & Shine, R. A. 2005, ApJ, 635, 659
Harvey, K., & Harvey, J. 1973, SoPh, 28, 61
Iida, Y., Hagenaar, H. J., & Yokoyama, T. 2012, ApJ, 752, 149
Jafarzadeh, S., Cameron, R. H., Solanki, S. K., et al. 2014, A&A, 563, A101
Kubo, M., Ichimoto, K., Shimitzu, T., Tsuneta, S., et al. 2007a, PASJ, 59, S607
Kubo, M., Shimizu, T., & Tsuneta, S. 2007b, ApJ, 659, 812
Martínez Pillet, V., Del Toro Iniesta, J. C., Álvarez-Herrero, A., et al. 2011a, SoPh, 268, 57
Sainz Dalda, A., & Martínez Pillet, V. 2005, ApJ, 632, 1176
Sheeley, N. R. 1969, SoPh, 9, 347
Shine, R., & Title, A. 2001, in Encyclopedia of Astronomy and Astrophysics, Vol. 4, ed. P. Murdin (London, Bristol: Nature Publishing, IOP Publishing), 3209
Solanki, S. K. 1987, PhD thesis, Eidgenössiche Technische Hochschule Zürich
Solanki, S. K., Barthol, P., Danilovic, S., et al. 2010, ApJL, 723, L127
Solanki, S. K., Riethmüller, T. L., Barthol, P., et al. 2017, ApJS, 229, 2
Title, A. M., Tarbell, T. D., Topka, K. P., et al. 1989, ApJ, 336, 475
Verma, M., & Balthasar, H., Deng, N., et al. 2012, A&A, 538, A109
Zhang, J., Solanki, S. K., & Wang, H. 2003, A&A, 399, 755
Zhang, J., Solanki, S. K., Woch, J., & Wang, J. 2007, A&A, 471, 1035
Zuccarello, F., Romano, P., Guglielmino, S. L., et al. 2009, A&A, 500, L5